DRAFT

BY

ROBERTO E. FAIRHURST AGOSTA

THESIS

Submitted in partial fulfillment of the requirements
for the degree of Master of Science in Nuclear, Plasma, Radiological Engineering
in the Graduate College of the
University of Illinois at Urbana-Champaign, 2020

Urbana, Illinois

Master's Committee:

Assistant Professor Kathryn D. Huff, Advisor
Professor Segundo Lector

# Abstract

Abstract.

# Acknowledgments

Acks.

# Table of Contents

**List of Tables** . . . . . **vi**

**List of Figures** . . . . . **vii**

**Chapter 1 Introduction** . . . . . **1**
1.1 The Prismatic High-Temperature Gas-Cooled Reactor . . . . . 1
1.2 Motivation . . . . . 3
1.3 Objectives . . . . . 4

**Chapter 2 Literature Review** . . . . . **6**
2.1 PMR neutronics . . . . . 6
2.2 PMR thermal-hydraulics . . . . . 6
2.3 PMR multi-physics . . . . . 6

**Chapter 3 Methodology** . . . . . **7**
3.1 Computational tools . . . . . 7
3.1.1 MOOSE . . . . . 7
3.1.2 Moltres . . . . . 8
3.1.3 Serpent . . . . . 8
3.2 Mathematical basis . . . . . 9
3.2.1 Diffusion and precursors equations . . . . . 9
3.2.2 Thermal-hydraulics . . . . . 10
3.3 OECD/NEA MHTGR-350 MW Benchmark . . . . . 11
3.4 MHTGR-350 Reactor Description . . . . . 12

**Chapter 4 Neutronics** . . . . . **16**
4.1 Preliminary studies . . . . . 16
4.2 OECD/NEA Benchmark . . . . . 16
4.3 Serpent-Moltres validation . . . . . 16

**Chapter 5 Thermal-hydraulics** . . . . . **17**
5.1 Preliminary studies . . . . . 17
5.2 Unit cell problem . . . . . 17
5.3 Fuel assembly . . . . . 17
5.4 Full core . . . . . 17

**Chapter 6 Hydrogen Production** . . . . . **18**
6.1 Introduction . . . . . 18
6.2 Illinois Climate Action Plan (iCAP) . . . . . 20
6.3 Objectives . . . . . 21
6.4 Hydrogen production methods . . . . . 21
6.4.1 Electrolysis . . . . . 21
6.4.2 Sulfur-Iodine Thermochemical Cycle . . . . . 23

6.5 Microreactors and Small Modular Reactors (SMRs) . . . 25
6.6 Methodology . . . 25
6.7 Results . . . 27
6.7.1 Transportation . . . 27
6.7.2 Electricity Generation . . . 29
6.8 Conclusions . . . 32

**Chapter 7 Conclusions . . . 34**
7.1 Contribution . . . 34
7.2 Future Work . . . 34

**References . . . 36**

# List of Tables

3.1 MHTGR350 Characteristics [40]. . . . . 13
3.2 MHTGR350 fuel element characteristics [40]. . . . . 14
3.3 TRISO and fuel compact characteristics [40]. . . . . 15
3.4 Lumped Burnable Poison (LBP) compact characteristics [40]. . . . . 15

6.1 Energy requirements of the different methods. . . . . 26
6.2 hydrogen ($H_2$) necessary to replace a gallon of fuel [45] [13]. . . . . 27
6.3 $H_2$ requirement for MTD and UIUC fleets. . . . . 27
6.4 carbon dioxide ($CO_2$) savings in lbs per gallon of fuel burned [1]. . . . . 28
6.5 $CO_2$ yearly savings. . . . . 28
6.6 Microreactor designs. . . . . 29

# List of Figures

1.1 Drawing of a TRISO fuel particle. Image reproduced from [22]. . . . . 2

3.1 MHTGR reactor layout. . . . . 13

6.1 Total United States (US) greenhouse gas (GHG) emissions by economic sector in 2017. Image reproduced from [20]. . . . . 18
6.2 The duck curve. Image reproduced from [8]. . . . . 19
6.3 Energy required by High-Temperature Electrolysis (HTE) at 3.5 MPa. . . . . 23
6.4 Diagram of the Sulfur-Iodine Thermochemical process. Image reproduced from [6]. . . . . 24
6.5 Energy required by the Sulfur-Iodine Thermochemical Cycle. . . . . 25
6.6 Diagram of a reactor coupled to a hydrogen plant. . . . . 26
6.7 Fuel consumption data. . . . . 27
6.8 $H_2$ requirement for MTD and UIUC fleets. . . . . 28
6.9 Hydrogen production rate by the different microreactor designs. . . . . 29
6.10 Prediction of the electricity generation in the US for 2050. Data from [2]. . . . . 30
6.11 Prediction of University of Illinois at Urbana-Champaign (UIUC)'s net demand for 2050. . . . . 30
6.12 $H_2$ production. . . . . 31
6.13 Peak reduction by using the produced $H_2$. . . . . 32

# Chapter 1

# Introduction

## 1.1 The Prismatic High-Temperature Gas-Cooled Reactor

The history of prismatic High-Temperature Gas-Cooled Reactors (HTGRs) or simply Prismatic Modular Reactors (PMRs) begins in the 1960s with the deployment of the Dragon reactor in the United Kingdom (UK). Its initial objective was to demonstrate the feasibility of the HTGR and launch the technology development. The Dragon reactor experiment first operated in July 1965 and reached full-power operation of 20 MWt in April 1966. The reactor operated for long periods at full power, demonstrated the successful operation of many components, and provided information on fuel and material irradiation tests. Simultaneously, interest in the US led to the 40 MWe HTGR at Peach Bottom. The reactor achieved initial criticality in March 1966 and went into commercial operation in June 1967. Peach Bottom provided demonstrated the HTGR concept by confirming the core physics calculations, verifying the design analysis methods, and providing a database for further design activities. Most importantly, the plant demonstrated the ability of HTGRs to function in a load-following manner [10]. After the deployment of these two prototype reactors came the first HTGR demonstration plant, the Fort St. Vrain (FSV) Generating Station. Its electric power generation started in December 1976, reaching full-power operation in November 1981. The FSV plant generated 842 MWt to achieve a net output of 330 MWe. This reactor laid the foundation for future prismatic designs. Beginning with FSV, the US core design included ceramic coated Tristructural Isotropic (TRISO) particles embedded within rods placed in large hexagonal shaped graphite elements [10].

The PMR's most fundamental characteristic is the unique safety philosophy embodied in its design [28]. The control of radionuclides does not rely on active systems or operator actions. TRISO particles, Figure 1.1, play a significant role in this task. They consist of various layers acting in concert to provide a containment structure that limits radioactive product release. A TRISO particle is a microsphere of about 0.8 mm in diameter. It includes a fuel kernel surrounded by a porous carbon layer (or buffer), followed successively by an inner pyrolitic carbon (IPyC) layer, a silicon carbide (SiC) layer, and an outer pyrolitic carbon (OPyC) layer. An additional advantage of the TRISO particles is that they increase the proliferation resistance of HTGRs. They are a very unattractive and the least desirable route for diversion or theft of weapons-usable materials [27].

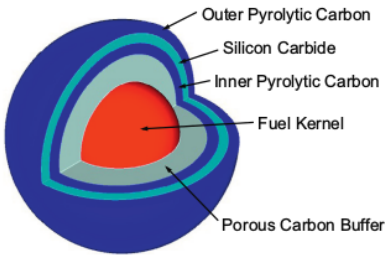


Figure 1.1: Drawing of a TRISO fuel particle. Image reproduced from [22].

Another contributor to the passive safety of the HTGR design is its materials. Combining a graphite core structure, ceramic fuel, and inert helium permits very high operating temperatures [5]. Graphite has a high heat capacity and maintains its strength at temperatures beyond 2760 °C. As a result, temperature changes in the core occur very slowly and without damage to the core structure during transients. Besides, the annular core geometry and a low core power density enable passive heat transfer mechanisms to remove the decay heat following postulated accidents [41]. These passive heat transfer mechanisms rely primarily on the natural processes of conduction, thermal radiation, and convection.

A desirable feature of the HTGR is its higher operating temperature. Higher temperatures offer increased cycle efficiencies. The early HTGR designs converted their heat into electricity using the Rankine steam cycle [26]. In such a system, the helium coolant passes through a heat exchanger generating steam to drive a turbine. This arrangement is around 38% efficient [9]. Some of these designs would superheat the steam to increase their efficiency, but this complicates the plant layout [5]. A practical temperature limit is around 300-400 °C. To take advantage of the high core outlet temperature of the HTGR, the Brayton cycle is a better option, where the helium coolant directly drives a gas turbine in a closed cycle. With such configuration, the system can achieve an energy conversion efficiency of around 48% [9]. Additionally, having helium circulating in a closed cycle removes external sources of contamination of the nuclear circuit. Thus, the need for on-line cleanup systems is vastly reduced [28].

Another advantage of the HTGR over other reactor designs is that higher outlet temperatures and increased cycle efficiencies enable a wide range of process heat applications. Some applications use steam for coal gasification processes, oil refinery processes, and synthesis gas production, methanol, and hydrogen. Several hydrogen production processes benefit from high temperatures. Some examples are high-temperature electrolysis or thermochemical water splitting. Utilizing the HTGR as the energy source of the process eliminates the need to burn fossil fuels to generate the steam those processes require [28].

This thesis focuses primarily on the Modular High-Temperature Gas-Cooled Reactor (MHTGR)-350 [41] [51]. Under the sponsorship of the US Department of Energy (DOE), a team consisting of General Atomics, Combustion Engineering, General Electric, Bechtel National, Stone & Webster Engineering, and Oak Ridge National Laboratory

(ORNL) developed the MHTGR [41]. They designed the basic module to deliver superheated steam at 17.3 MPa and 538 °C. Based on both economic and technological considerations, a 350 MWt modular reactor defines the optimal configuration. The team completed in 1986 the preliminary safety information document for the MHTGR and the complete draft pre-application in 1989 [27].

## 1.2 Motivation

This work's ultimate goal is to support the development of HTGR technology. More specifically, we focus on the development of computational methods for modeling HTGRs. We use *Moltres* as our primary analysis tool.

The Generation IV Roadmap project identified reactor concepts that could meet the future's energy demands in an efficient, economical, and environmentally safe manner [36]. One of these reactor concepts is the Very High Temperature Gas Cooled Reactor (VHTR). VHTR is distinct from HTGR as its coolant outlet temperature reaches higher temperatures. However, the literature often uses these terms interchangeably. In this work, the term HTGR encompasses both terms. The DOE had selected this reactor concept for the Next Generation Nuclear Power (NGNP) Project. This project intended to demonstrate emissions-free nuclear-assisted electricity and hydrogen production by 2015.

Although the DOE has canceled the NGNP Project, HTGRs will become a reality in the near term. Some microreactor designs embody this type of technology and may be operational before 2030. Additionally, as the introduction has already described, the HTGR technology has several favorable characteristics. To recapitulate the most important features, the HTGR relies on passive heat transfer mechanisms, uses TRISO particles as its fuel, has a high proliferation resistance, can achieve high temperatures, and benefits from increased cycle efficiencies. Other beneficial characteristics are that high temperatures enable a wide range of process heat applications, among which we find hydrogen production.

Modeling and prediction of core thermal-hydraulic behavior is necessary for assessing the safety characteristics of a reactor. Determining the temperature inside a reactor, for both normal and transient operation, is of paramount importance as the several materials' integrity depends on it. Most importantly, undesirably high temperatures endanger the TRISO particles' integrity and, consequently, jeopardize a fission product release [53]. Furthermore, the fuel blocks' complex geometry hinders accurate calculations of the fuel temperatures requiring elaborate numerical calculations.

The characteristics of an HTGR are different from those of conventional Light Water Reactors (LWRs). Such differences create a demand for new reactor analysis tools. These new tools should take into account the following peculiarities of HTGRs [50][7]:

- Hexagonal structure: the shape of the fuel blocks does not conform to any orthogonal coordinate system.
- Double heterogeneity: the TRISO particles form the first heterogeneity level, consisting of four layers. The second level arises from the fuel elements, as they encompass the compacts, the coolant, and the moderator.
- Strong dependence of the neutron spectrum and the macroscopic cross-sections on the fuel temperatures.
- The high thermal inertia of the reactor core causes long transients due to large graphite structures.

Historically, linking a stand-alone neutronics solver to a thermal-hydraulics solver allowed for simulating an entire reactor. The coupling of the codes occurred in a black-box fashion, where one code's output served as the other's input, and vice versa. This coupling technique is commonly known as the operator-splitting technique [49]. In such an approach, each individual physics isolates the action of the governing equations upon the variables. Nonetheless, these physical models describe processes that rely heavily on the solution of one another's. The neutron flux determines the power distribution. The power distribution has a strong influence on the temperature field. Due to the HTGR strong temperature feedback, the temperature affects the neutron flux distribution in the core. Because of a large time-scale separation between the different phenomena, multiphysics transient simulations coupled via the operator-splitting approach may introduce significant numerical errors [49] [48].

Multiphysics Object-Oriented Simulation Environment (MOOSE) [21] is a computational framework targeted at solving fully coupled systems. All the software built on the MOOSE framework shares a joint code base. These features facilitate relatively easy coupling between different phenomena and allow for great flexibility, even with a large variance in time scales [42]. Additionally, all codes use MPI for parallel communication and allow for deployment on massively-parallel cluster-computing platforms.

*Moltres* [35] is a Finite Element Method (FEM) simulation code built within the MOOSE framework. *Moltres* solves arbitrary-group neutron diffusion, precursor, and temperature governing equations. Besides, this simulation tool is open source. All these characteristics make *Moltres* suitable for solving the type of physical phenomena described above.

## 1.3 Objectives

As mentioned earlier, the ultimate goal of this work is to support the development of HTGR technology. The following list of main objectives expands on that goal.

**Extend Moltres modeling capabilities to HTGRs.** Moltres is a multi-physics solver of Molten Salt Reactor (MSR). Enhancing Moltres will allow it to model HTGRs as well.

**Couple the different physics phenomena present in an HTGR.** Moltres's current capabilities allow for solving some of the physics in the HTGR design. Nevertheless, the inherent physics in an HTGR needs to be captured by the solver and adequately integrated into the current capabilities.

**Develop safety analysis capabilities in Moltres.** Steady-state simulations help understand the fundamental behavior of an HTGR. They are also necessary for reactor design. Transient simulations are also necessary for reactor design. Transient simulations assess the reactor response in design basis events.

**Understand HTGR contribution to stopping climate change.** HTGRs are capable of attaining high temperatures. Such feature makes them attractive for deployment alongside hydrogen plants. With high temperatures, the efficiency of hydrogen production increases.

The main objectives are somewhat broad. The following list presents secondary objectives that will lead to the fulfillment of the main objectives:

**Predict neutronics appropriately.** Moltres should have the ability to carry out eigenvalue calculations appropriately. Additionally, Moltres should predict the flux shape and magnitude accurately, during steady-state and transient simulations.

**Understand the impact of some simulation parameters.** The underlying physics of HTGRs are different from the physics of other reactors. Consequently, the simulation results will be sensitive to different parameters from other reactor type simulations. This work will focus on the energy group structure and its effects on the diffusion calculations. We will also assess the effect of such parameters on the performance of the simulations.

**Calculate power distribution correctly.** The importance of an accurate neutronics behavior prediction lies in the accurate prediction of the power distribution. The power distribution is the most influential parameter over the thermal-hydraulics as it determines the temperature profile in the reactor.

**Predict temperature profile accurately.** Undesirably high temperatures endanger the integrity of the TRISO particles. Additionally, the temperature influences the neutronics. Hence, an accurate neutronics calculation will not be accurate without an accurate thermal-hydraulics calculation, and vice versa.

**Develop a hydrogen production calculation tool.** There exist several production methods. Most of them have different energy requirements and have different production rates. We will develop a tool to determine such quantities.

# Chapter 2

# Literature Review

## 2.1 PMR neutronics

This section will talk about deterministic diffusion solvers and related past studies.

## 2.2 PMR thermal-hydraulics

This section will talk about thermal-hydraulic calculations in prismatic HTGRs and related past studies.

## 2.3 PMR multi-physics

This section will talk about previous efforts on multi-physic couplings for prismatic HTGRs.

# Chapter 3

# Methodology

## 3.1 Computational tools

### 3.1.1 MOOSE

MOOSE[21] is a computational framework whose purpose is to support engineering analysis applications. In a nuclear reactor, several Partial Differential Equations (PDEs) describe its physical behavior. These equations are typically nonlinear, and they are often strongly coupled to each other. MOOSE targets such systems and solves them in a fully coupled manner.

MOOSE is an open-source code under a Lesser GNU Public License (LGPL). The code itself relies on LibMesh [31], an LGPL finite element library, and PetSc, a Berkeley Software Distribution (BSD)-licensed toolkit for solving nonlinear equations [4]. MOOSE applications define weak forms of the governing equations. They modularize the physics expressions into "Kernels." Kernels are C++ classes containing methods for computing the residual and Jacobian contributions of individual pieces of the governing equations. MOOSE and LibMesh translate them into residual and Jacobian functions. These functions become inputs into PetSc solution routines.

MOOSE utilizes the mathematical structure present in Jacobian-Free Newton-Krylov (JFNK) methods [32]. JFNK methods are synergistic combinations of Newton-type methods for superlinearly convergence of nonlinear equations and Krylov subspace methods for solving the Newton correction equations. The link between the two methods is the Jacobian-vector product. JFNK methods compute such products approximately without forming and storing the elements of the true Jacobian. The ability to perform a Newton iteration without forming the Jacobian gives JFNK methods potential for application throughout problems governed by nonlinear partial differential equations.

All the software built on the MOOSE framework shares a joint code base. The applications, by default, use monolithic and implicit methods. This feature facilitates relatively easy coupling between different phenomena and allows for great flexibility, even with a large variance in time scales [42]. Additionally, all codes use MPI for parallel communication and allow for deployment on massively-parallel cluster-computing platforms.

### 3.1.2 Moltres

*Moltres* [35] is a MOOSE based application initially designed for modeling fluid-fuelled MSRs. This simulation tool is open source and counts with an LGPL license. It uses `git` for version control, emphasizing its openness and promoting quality through peer review.

Moltres solves arbitrary-group neutron diffusion, precursors, and temperature governing equations. It can solve the equations in a fully-coupled way or solve each system independently, allowing for great flexibility and making it applicable to a wide range of nuclear engineering problems.

### 3.1.3 Serpent

The Serpent Monte Carlo code [33] [34] is a three-dimensional continuous-energy neutron transport code. VTT Technical Research Centre of Finland developed it, and it has been in public distribution since 2009. Monte Carlo neutron transport codes have several reactor physics applications related to criticality safety analyses, radiation shielding problems, detector modeling, and validation of deterministic transport codes. The Monte Carlo method's main advantage is its capability to model geometry and interaction physics without significant approximations. The main disadvantage is that modeling complex systems are very computing-intensive, restricting the applications to some extent.

Serpent serves two primary purposes: (1) reactor modeling, and (2) group constant generation. In reactor modeling, the Monte Carlo simulation itself represents the solution to the full-scale problem. In group constant generation, the transport simulation produces input parameters for a deterministic code. Based on a few groups, deterministic codes allow for carrying out coupled full-core analyses.

In this work, Serpent produces group constants that serve as an input for Moltres and solves the heterogeneous system. This last step provides the reference solutions for the validation of the Moltres calculation scheme. For the calculations, we used Serpent 2.1.31 and the cross-section library JEFF3.1.2. The choice of Serpent as the cross-section generation tool comes from one of its capabilities. Serpent allows for the explicit modeling of randomly located TRISO particles. Applying a simple volume homogenization has proven inaccurate due to the resonant self-shielding effect of the kernel and coated layers. Although the particles' explicit modeling is time-consuming, costly, and impractical for most applications, it results necessary.

## 3.2 Mathematical basis

### 3.2.1 Diffusion and precursors equations

Equations 3.1 and 3.2 describe the time dependent behavior of the neutronics.

$$\frac{1}{v_g}\frac{\partial}{\partial t}\phi_g = \nabla \cdot D_g \nabla \phi_g - \Sigma_g^r \phi_g + \sum_{g \neq g'}^{G} \Sigma_{g' \to g}^s \phi_{g'} + \chi_g^p \sum_{g'=1}^{G} (1-\beta) \nu \Sigma_{g'}^f \phi_{g'} + \chi_g^d \sum_{i}^{I} \lambda_i C_i \tag{3.1}$$

$$\frac{\partial}{\partial t} C_i = \sum_{g'=1}^{G} \beta_i \nu \Sigma_{g'}^f \phi_{g'} - \lambda_i C_i \tag{3.2}$$

where

$$\begin{aligned}
v_g &= \text{group } g \text{ neutron speed} \\
\phi_g &= \text{group } g \text{ neutron flux} \\
t &= \text{time} \\
D_g &= \text{group } g \text{ diffusion coefficient} \\
\Sigma_g^r &= \text{group } g \text{ macroscopic removal cross-section} \\
\Sigma_{g' \to g}^s &= \text{group } g' \text{ to group } g \text{ macroscopic scattering cross-section} \\
\chi_g^p &= \text{group } g \text{ prompt fission spectrum} \\
G &= \text{number of discrete energy groups} \\
\nu &= \text{number of neutrons produced per fission} \\
\Sigma_g^f &= \text{group } g \text{ macroscopic fission cross-section} \\
\chi_g^d &= \text{group } g \text{ delayed fission spectrum} \\
I &= \text{number of delayed neutron precursor groups} \\
\beta &= \text{delayed neutron fraction} \\
\lambda_i &= \text{average decay constant of delayed neutron precursors in precursor group } i \\
C_i &= \text{concentration of delayed neutron precursors in precursor group } i.
\end{aligned} \tag{3.3}$$

We apply the vacuum boundary condition to the diffusion equation. The vacuum boundary condition states that no neutrons penetrate the boundary in the inward direction. In other words, the incoming current density

($J^-(r_s,t)$) is equal to zero, equation 3.4 [17].

$$J^-(r_s,t) = \frac{1}{4}\phi(r_s,t) + \frac{D}{2}\hat{n_s}\cdot\nabla\phi(r_s,t) = 0 \tag{3.4}$$

### 3.2.2 Thermal-hydraulics

The governing equation for the temperature of the solids is the three-dimensional heat conduction equation [37]. Equations 3.5 to 3.7 allow for solving the temperature in the fuel, moderator, and reflector.

$$\rho_i c_{p,i}\frac{\partial}{\partial t}T_i = k_i\nabla^2 T_i + Q_i \tag{3.5}$$

$$Q_f = \sum_{g=1}^{G}\epsilon_g^f\Sigma_g^f\phi_g \tag{3.6}$$

$$Q_m = Q_r = 0 \tag{3.7}$$

where

$i$ = f (fuel), m (moderator), r (reflector)

$\rho_i$ = material $i$ density

$c_{p,i}$ = material $i$ heat capacity

$k_i$ = material $i$ thermal conductivity

$T_i$ = material $i$ temperature

$Q_i$ = material $i$ volumetric heat source

$\epsilon_g^f$ = energy released per fission

$\Sigma_g^f$ = group $g$ macroscopic fission cross-section

$\phi_g$ = group $g$ neutron flux.

The governing equation of the coolant is the one-dimensional form of the continuity, momentum, and energy conservation equations, equations 3.8 to 3.12 [59][52].

$$\frac{\partial}{\partial t}\rho_c + \nabla \cdot (\rho_c u) = 0 \tag{3.8}$$

$$\rho_c \left( \frac{\partial}{\partial t} u + u \frac{\partial}{\partial z} u \right) = -\frac{\partial}{\partial z} p - \tau \frac{\varepsilon}{A} - \rho_c g \tag{3.9}$$

$$\rho_c \left( \frac{\partial}{\partial t} (c_{p,c} T_c) + u \frac{\partial}{\partial z} (c_{p,c} T_c) \right) = \frac{\partial}{\partial t} p + u \frac{\partial}{\partial z} p + q'''_{conv} \tag{3.10}$$

$$\tau = \frac{f}{2} \rho_c u^2 \tag{3.11}$$

$$q'''_{conv} = h \frac{\varepsilon}{A} (T_i - T_c) \tag{3.12}$$

where

$\rho_c$ = coolant density

$u$ = coolant velocity

$p$ = coolant pressure

$\tau$ = shear stress

$\varepsilon$ = wetted perimeter

$A$ = cross-sectional area

$g$ = gravity

$c_{p,c}$ = coolant specific heat capacity

$T_c$ = coolant temperature

$k_c$ = coolant thermal conductivity

$q'''_{conv}$ = convective heat transfer

$f$ = friction factor

$h$ = heat transfer coefficient

$T_i$ = solid temperature.

## 3.3 OECD/NEA MHTGR-350 MW Benchmark

The deterministic neutronic thermal-fluids and transient analysis methods available for prismatic HTGRs have lagged behind the state of the art of other reactor technologies. This delay has motivated the development of more

accurate tools for the design and safety evaluations of HTGRs. In addition to the development of new methods, it is essential to define appropriate benchmarks to compare these new methods' capabilities. The Organisation for Economic Co-operation and Development (OECD)/Nuclear Energy Agency (NEA) defined such a benchmark [40] using the MHTGR-350 MW reactor [51] as the reference design. The scope of the benchmark is twofold: (1) to establish a well-defined problem, based on a common given data set, to compare methods and tools in core simulation and thermal fluids analysis, and (2) to test the depletion capabilities of various lattice physics codes available for prismatic HTGRs.

The benchmark defines several Phases and Exercises:

- Phase I: Steady State
    1. Neutronics solution with fixed cross-sections.
    2. Thermal fluids solution with given heat sources.
    3. Coupled neutronics-thermal fluids steady state solution.
- Phase II: Transient Cases
    1. Depressurized Conduction Cooldown without reactor trip.
    2. Pressurized Conduction Cooldown with reactor trip.
    3. Water ingress with reactor trip.
    4. Power 100-80-100 load follow.
- Phase III: Lattice Depletion Case

## 3.4 MHTGR-350 Reactor Description

This section describes the MHTGR-350 reactor. Table 3.1 lists its main characteristics. The core consists of an array of hexagonal fuel elements in a cylindrical arrangement, Figure 3.1. Nineteen graphite replaceable reflector elements compose the inner reflector region. A ring of identically sized graphite replaceable reflector elements surrounds the fuel elements. Then, a region of permanent reflector elements follows the replaceable reflectors. The reactor vessel encases all the elements.

Ten layers of fuel elements stacked on top of each other compose the 66 fuel columns that integrate the active core. Figure 3.1b shows an axial view of the reactor. The core has two types of fuel elements: a standard element and a reserve shutdown element that contains a channel for Reserve Shutdown Control (RSC). Table 3.2 specifies the details of the MHTGR-350 fuel elements. Twelve columns in the core contain RSC channels for reserve shutdown

Table 3.1: MHTGR350 Characteristics [40].

| Characteristics | Value |
|---|---|
| Installed Thermal Capacity | 350 MWt |
| Installed Electric Capacity | 165 MWe |
| Core inlet/outlet Temperature | 259/687°C |
| Power Density | 5.9 MW/m$^3$ |
| Reactor Vessel Outside diam. | 6.8 m |
| Reactor Vessel Height | 22 m |
| Active core radius | 2.97 m |
| Active core height | 7.93 m |
| Top reflector height | 1.18 m |
| Bottom reflector height | 1.98 m |
| Number of fuel columns | 66 |
| Number of inner reflector columns | 19 |
| Number of outer reflector columns | 78 |

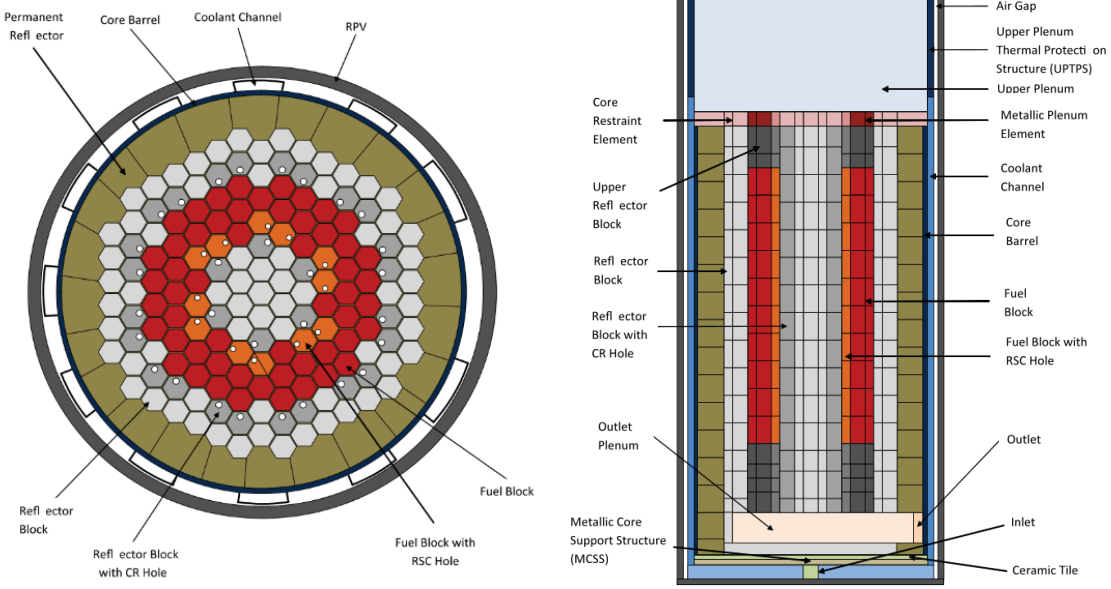


(a) Core radial layout. Image reproduced from [40].

(b) Core axial layout. Image reproduced from [40].

Figure 3.1: MHTGR reactor layout.

borated graphite pellets. Hoppers above the core house the pellets, and if the control rods (CRs) become inoperable, the pellets drop into the channels [40].

Table 3.2: MHTGR350 fuel element characteristics [40].

| Shared characteristics | Value | Units |
|---|---|---|
| Block pitch (flat-to-flat) | 36 | cm |
| Fuel length | 79.3 | cm |
| Fuel handling diameter | 3.5 | cm |
| Fuel handling length | 26.4 | cm |
| RSC hole diameter | 9.525 | cm |
| RSC center to assembly center | 9.756 | cm |
| Fuel/coolant pitch | 1.879 | cm |
| Fuel hole radius | 0.635 | cm |
| Compacts per fuel hole | 15 | - |
| Large coolant hole radius | 0.794 | cm |
| Small coolant hole radius | 0.635 | cm |
| LBP hole radius | 0.635 | cm |
| Block graphite density | 1.85 | $g/cm^3$ |
| Standard element | | |
| Number of large coolant holes | 120 | - |
| Number of small coolant holes | 6 | - |
| Number of fuel holes | 210 | - |
| RSC element | | |
| Number of large coolant holes | 88 | - |
| Number of small coolant holes | 7 | - |
| Number of fuel holes | 186 | - |

The fuel elements contain blind holes for fuel compacts and full-length channels for helium coolant flow. Table 3.3 specifies the details of the TRISO particle and fuel compact designs of the MHTGR-350.

A combination of LBP and CRs controls the core reactivity. The LBP consists of boron carbide (B4C) granules dispersed in graphite compacts. The current design uses six LBP rods per element. Table 3.4 displays the characteristics of the LBP compacts. The reactor counts with 30 CRs. Six of them are start-up CRs, and their location is the inner reflector. The remaining 24 are operating CRs and control the reactivity during power operation and a reactor trip.

Table 3.3: TRISO and fuel compact characteristics [40].

| Characteristic | Value | Units |
|---|---|---|
| Fuel | $UC_{0.5}O_{1.5}$ | - |
| Enrichment (average) | 15.5 | wt% |
| Packing fraction (average) | 0.35 | - |
| Kernel radius | 0.021,25 | cm |
| Buffer radius | 0.031,25 | cm |
| IPyC radius | 0.034,75 | cm |
| SiC radius | 0.038,25 | cm |
| OPyC radius | 0.042,25 | cm |
| Compact radius | 0.622,5 | cm |
| Compact gap radius | 0.635,0 | cm |
| Compact length | 4.928,0 | cm |
| Kernel density | 10.50 | $g/cm^3$ |
| Buffer density | 1.00 | $g/cm^3$ |
| IPyC density | 1.90 | $g/cm^3$ |
| SiC density | 3.20 | $g/cm^3$ |
| OPyC density | 1.90 | $g/cm^3$ |
| Compact matrix density | 1.74 | $g/cm^3$ |

Table 3.4: LBP compact characteristics [40].

| Characteristic | Value | Units |
|---|---|---|
| Absorber | $B_4C$ | - |
| Packing fraction | 0.109 | - |
| Kernel radius | 0.010,0 | cm |
| Buffer radius | 0.011,8 | cm |
| PyC radius | 0.014,1 | cm |
| Compact radius | 0.571,5 | cm |
| Compact gap radius | 0.635,0 | cm |
| Rod length | 72.187 | cm |
| Kernel density | 2.47 | $g/cm^3$ |
| Buffer density | 1.00 | $g/cm^3$ |
| PyC density | 1.87 | $g/cm^3$ |
| Compact matrix density | 0.94 | $g/cm^3$ |

# Chapter 4

# Neutronics

## 4.1 Preliminary studies

This section will discuss the current capabilities in Moltres and discuss its applicability to PMRs.

## 4.2 OECD/NEA Benchmark

This section solves the Exercise 1 of Phase I of the OECD/NEA MHTGR-350 benchmark with the current Moltres capabilities.

## 4.3 Serpent-Moltres validation

This section compares the results from Moltres and Serpent. Serpent generates the homogenized group constants and also solves the heterogeneous system, which provides the reference solutions for the validation of the calculation scheme.

# Chapter 5

# Thermal-hydraulics

## 5.1 Preliminary studies

This section carries out some preliminar studies using Moltres and MOOSE heat conduction module.

## 5.2 Unit cell problem

This section will solve the unit cell problem in the hot spot of an HTGR.

## 5.3 Fuel assembly

This section will calculate the heat profile of a fuel assembly of a HTGR.

## 5.4 Full core

This section will extend the methodology to a fullcore problem and it will inted to solve Exercise 2 of Phase I of the OECD/NEA MHTGR-350 Benchmark.

# Chapter 6

# Hydrogen Production

## 6.1 Introduction

Energy is one of the most vital contributors to economic growth. In the future, economies will continue to expand, populations will do so too, and their energy demand will accompany such change [12] [18]. Meeting these future needs requires the development of clean energy sources as environmental concerns continue to rise.

As seen in Figure 6.1, electricity generation was one of the economic sectors that released the most GHGs in the US in 2017. As $CO_2$ is the main component in GHGs, decarbonizing electricity generation will allow us to meet the increases in energy demand and address the environmental concerns simultaneously.

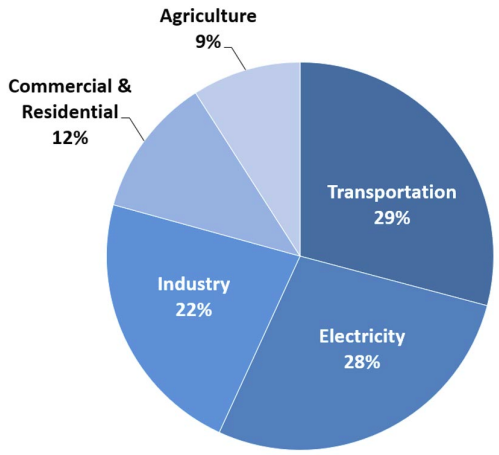


Figure 6.1: Total US GHG emissions by economic sector in 2017. Image reproduced from [20].

To address these concerns, utility companies are relying more and more on renewable energy resources, such as wind and solar [38]. However, high solar adoption creates a challenge. The need for electricity generators to quickly ramp up increases when the sun sets and the contribution from the photovoltaics (PV) falls [44]. The "duck curve" (or duct chart) depicts this phenomenon, Figure 6.2. The California ISO (CAISO) developed the duck curve to illustrate the grid's net load [8]. We define the net load as the difference between forecasted load and expected electricity production from solar.

Moreover, the duck curve reveals another issue. Over-generation may occur during the middle of the day, and high-levels of non-dispatchable generation may exacerbate the situation. As a consequence, the market would experience sustained zero or negative prices during the middle of the operating day [8].

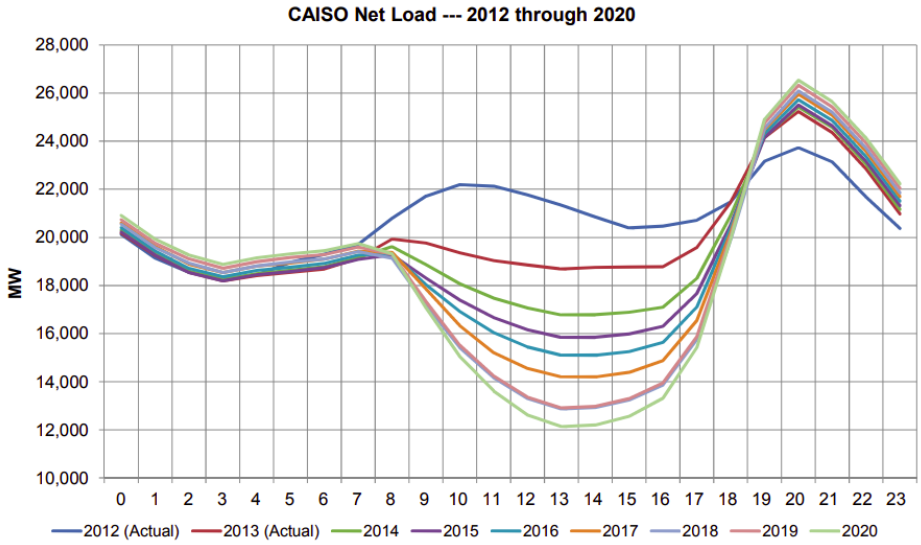


Figure 6.2: The duck curve. Image reproduced from [8].

The simplest solution to a demand ramp-up is to increase dispatchable generation, resources with fast ramping and fast starting capabilities such as natural gas and coal [8], and, consequently, decrease non-dispatchable generation, such as geothermal, nuclear, and hydro. Nonetheless, an approach like this is not consistent with the goal of reducing carbon emissions. Hence, our focus drifts to other potential low-carbon solutions, like nuclear generation and electricity storage through $H_2$ production.

Unfortunately, a carbon-neutral electric grid will be insufficient to halt climate change because transportation is a significant contributor to GHG emissions. As seen in Figure 6.1, transportation released the most GHGs in the US in 2017. Thus, decarbonizing transportation underpins global carbon reduction. One possible strategy is to develop a hydrogen economy, as Japan is currently doing. Japan's strategy rests on the firm belief that $H_2$ can be a decisive response to its energy and climate challenges. It could foster deep decarbonization of the transport, power, industry, and residential sectors while strengthening energy security [39]. In the transportation sector, Japan plans to deploy fuel cell vehicles, trucks, buses, trains, and ships.

Although $H_2$ technologies do not release $CO_2$, any $H_2$ production method is only as carbon-free as the energy source it relies on (electric, heat, or both). Nuclear reactors introduce a clean energy option to manufacture $H_2$.

The UIUC is leading by example and actively working to reduce GHG emissions from electricity generation and transportation (among other sectors) on its campus. In pursuance of those efforts, the university has developed the iCAP.

## 6.2 iCAP

In 2008, UIUC signed the American College and University Presidents' Climate Commitment, formally committing to becoming carbon neutral as soon as possible, no later than 2050. The university developed the first iCAP in 2010 as a comprehensive roadmap toward a sustainable campus environment [46]. The iCAP defines a list of goals, objectives, and potential strategies for six topical areas.

- Energy Conservation and Building Standards:

Focuses on maintaining or reducing campus gross square footage, strengthen conservation efforts, and engage the campus community in energy conservation.

- Energy Generation, Purchasing, and Distribution:

Efforts towards the exploration of 100% clean campus energy options. This includes expanding on-campus solar energy production, the extension of the purchase of clean energy from low-carbon energy sources, and the offset of all emissions from the National Petascale Computing Facility.

- Transportation:

This area comprises the efforts to reduce air travel emissions, reduce Urbana-Champaign campus fleet emissions, and study scenarios for complete conversion of the campus fleet to renewable fuels.

- Water and Stormwater:

This area focuses on improving the water efficiency of cooling towers, perform a water audit to establish water conservation targets, determine upper limits for water demand by end-use, and implement projects to showcase the potential of water and stormwater reuse.

- Purchasing, Waste, and Recycling:

Attempt to standardize office paper purchases, cleaning products, computers, other electronics, and freight delivery services. It also attempts to foment recycling by reducing non-durable goods purchases and reducing municipal solid waste going to landfills.

- Agriculture, Land Use, Food, and Sequestration:

This area will perform a comprehensive assessment of GHG emissions from agricultural operations, and develop a plan to reduce them, implement a project that examines the foodservice carbon footprint for Dining, and increase carbon sequestration in campus soils.

## 6.3 Objectives

As mentioned earlier, we place our attention on two areas: electricity generation and transportation. We will turn our attention to electricity generation and transportation on the UIUC campus. Consequently, this work's objective aligns with the efforts in two of the six target areas defined on the iCAP.

Regarding electricity generation, our analysis focuses on the UIUC grid. The present work quantifies the magnitude of the duck curve in such a grid. To mitigate the risk of over-generation, we propose to use the over-generated energy to manufacture $H_2$. We chose a nuclear reactor to be the primary source of energy. The next step is to quantify how much $H_2$ different production methods can produce. Section 6.4 discusses a few hydrogen production methods considered for our analysis. Finally, we will calculate how much electricity we would generate using the $H_2$ produced.

Regarding transportation, we study the conversion of the UIUC fleet on campus to Fuel Cell Electric Vehicles (FCEVs). Additionally, the analysis includes the conversion of the Champaign-Urbana Mass Transit District (MTD) fleet as well. The first step is to determine the fuel consumed by both fleets and how much $H_2$ enables the fleets' complete conversion. Finally, we consider a few reactor designs and analyze which of them could produce enough $H_2$ to fulfill both fleet requirements.

Both studies propose the same solution, a nuclear reactor coupled to a hydrogen plant. In terms of electricity generation, this solution will decrease the need for dispatchable sources and, consequently, reduce carbon emissions. In terms of transportation, it will eliminate carbon emissions.

In both analyses, many reactor choices can satisfy our needs. The typical UIUC's grid demand is smaller than 80 MW [16]. Accordingly, we consider reactors of small capacities, such as microreactors and SMRs. Section 6.5 discusses their characteristics.

## 6.4 Hydrogen production methods

This section introduces several hydrogen production processes and their energy requirements.

### 6.4.1 Electrolysis

The electrolysis of water is a well-known method whose commercial use began in 1890. This process produces approximately 4% of $H_2$ worldwide. The process is ecologically clean because it does not emit GHGs. However, in comparison with other methods, electrolysis is a highly energy-demanding technology [30].

Three electrolysis technologies exist. Alkaline-based is the most common, the most developed, and the lowest in capital cost. It has the lowest efficiency and, therefore, the highest electrical energy cost. Proton exchange

membrane electrolyzers are more efficient but more expensive than Alkaline electrolyzers. Solid Oxide Electrolysis Cells (SOEC) electrolyzers are the most electrically efficient but the least developed. SOEC technology has challenges with corrosion, seals, thermal cycling, and chrome migration [30]. As the first two technologies work with liquid water and the latter requires high-temperature steam, we will refer to the first two as Low-Temperature Electrolysis (LTE) and the latter as HTE.

Water electrolysis converts electric and thermal energy into chemical energy stored in hydrogen. The process enthalpy change $\Delta H$ determines the required energy for the electrolysis reaction to take place. Part of the energy corresponds to electric energy $\Delta G$ and its rest to thermal energy $T \cdot \Delta S$, Equation 6.1.

$$\Delta H = \Delta G + T\Delta S \tag{6.1}$$

where

$$\Delta H = \text{Total specific energy [kWh/kg-H}_2\text{]} \tag{6.2}$$

$$\Delta G = \text{Specific electrical energy [kWh/kg-H}_2\text{]} \tag{6.3}$$

$$T\Delta S = \text{Specific thermal energy [kWh/kg-H}_2\text{]}. \tag{6.4}$$

In LTE, electricity generates thermal energy. Hence, $\Delta H$ alone determines the process required energy. $\Delta H$ is equal to 60 kWh/kg-$H_2$ considering a 67% efficiency [56].

In HTE, a high-temperature heat source is necessary to provide thermal energy. $\Delta G$ decreases with increasing temperature, Figure 6.3. Decreasing the electricity requirement results in higher overall production efficiencies since heat-engine-based electrical work has a thermal efficiency of 50% or less [29]. Figure 6.3 shows $\Delta G$ and $T\Delta$S. $\Delta G$ considers the SOEC to have an electrical efficiency of 88% [24]. $T\Delta S$ accounts for the latent heat of water vaporization. Note that the process is at 3.5 MPa. $\Delta G$ increases with pressure. However, we chose a high pressure to save energy, as compressing liquid water is cheaper than compressing the hydrogen [47].

Finally, equations 6.5 and 6.6 determine the electrical $P_{EH2}$ and thermal power $P_{TH2}$ required by the hydrogen plant.

$$P_{EH2} = \dot{m}_{H2}\Delta G \tag{6.5}$$

$$P_{TH2} = \dot{m}_{H2} T\Delta S \tag{6.6}$$

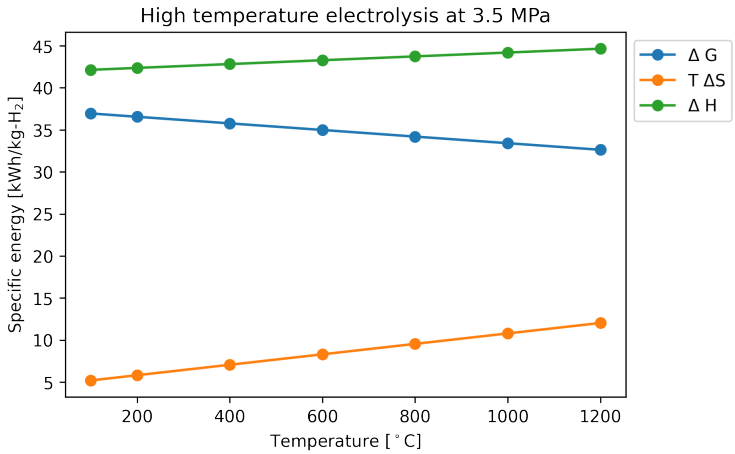


Figure 6.3: Energy required by HTE at 3.5 MPa.

where

$$P_{EH2} = \text{Total electrical power [kW]} \tag{6.7}$$

$$P_{TH2} = \text{Total thermal power [kW]} \tag{6.8}$$

$$\dot{m}_{H2} = \text{H}_2 \text{ production rate [kg/h]}. \tag{6.9}$$

### 6.4.2 Sulfur-Iodine Thermochemical Cycle

Thermochemical water-splitting is converting water into hydrogen and oxygen by a series of thermally driven chemical reactions. The direct thermolysis of water requires temperatures above 2500 °C for significant hydrogen generation. At this temperature, the process can decompose a 10% of the water. A thermochemical water-splitting cycle accomplishes the same overall result using much lower temperatures.

General Atomics, Sandia National Laboratories, and the University of Kentucky compared 115 cycles that would use high-temperature heat from an advanced nuclear reactor [11]. The report specifies a set of screening criteria used to rate each cycle. The highest scoring method was the Sulfur-Iodine (SI) Cycle.

The SI cycle consists of the three chemical reactions represented in Figure 6.4. The whole process takes in water and high-temperature heat and releases hydrogen and oxygen. The process does not use any electricity. The process recycles all reagents and does not have any effluents [60]. The chemical reactions are:

$$I_2 + SO_2 + 2H_2O \rightarrow 2HI + H_2SO_4 \tag{6.10}$$

$$H_2SO4 \rightarrow SO_2 + H_2O + 1/2O_2 \tag{6.11}$$

$$2HI \rightarrow I_2 + H_2. \tag{6.12}$$

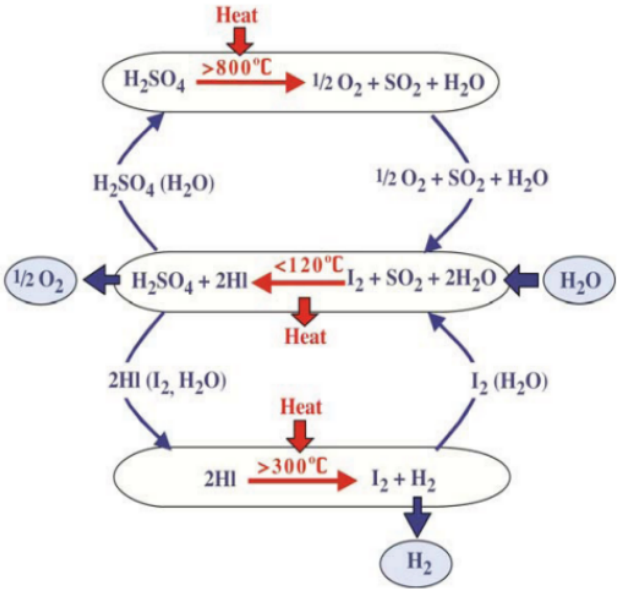


Figure 6.4: Diagram of the Sulfur-Iodine Thermochemical process. Image reproduced from [6].

Figure 6.5 presents the specific energy requirements of the cycle $\Delta H$. Several sources disagree on the minimum temperature for the process to be viable. Our analysis considers the process feasible only for temperatures above 800 °C. Finally, equation 6.13 determines the thermal power $P_{TH2}$ required by the hydrogen plant.

$$P_{TH2} = \dot{m}_{H2}\Delta H \tag{6.13}$$

where

$$P_{TH2} = \text{Total thermal power [kW]} \tag{6.14}$$

$$\dot{m}_{H2} = \text{H}_2 \text{ production rate [kg/h]} \tag{6.15}$$

$$\Delta H = \text{Specific energy [kWh/kg-H}_2\text{]}. \tag{6.16}$$

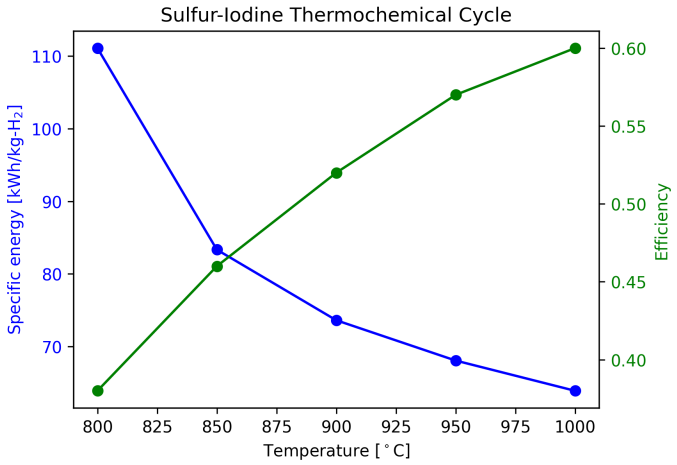


Figure 6.5: Energy required by the Sulfur-Iodine Thermochemical Cycle.

## 6.5 Microreactors and SMRs

These reactor concepts share several features. The reactors require limited on-site preparation as their components are factory-fabricated and shipped out to the generation site. This feature reduces up-front capital costs, enables rapid deployment, and expedites start-up times. This reactor concept allows for black starts and islanding operation mode. They can start up from an utterly de-energized state without receiving power from the grid. They can also operate connected to the grid or independently. Moreover, these types of reactors are self-regulating. They minimize electrical parts and use passive safety systems to prevent overheating and safely shutdown.

Microreactors have the distinction that is transportable. Small designs make it easy for vendors to ship the entire reactor by truck, shipping vessel, or railcar. These features make the technology appealing for a wide range of applications, such as deployment in remote residential locations and military bases.

The DOE defines a microreactor as a reactor that generates from 1 to 20 MWt [55]. The International Atomic Energy Agency (IAEA) describes an SMR as a reactor whose power is under 300 MWe. It defines, as well, a very small modular reactor as a reactor that produces less than 15 MWe [3]. As the definitions of these reactor concepts overlap, we will consider reactors of less than 100 MWt regardless of their specific classification.

## 6.6 Methodology

In this analysis, the energy source (electric and thermal) is a nuclear reactor with co-generation capabilities. The nuclear reactor supplies the grid with electricity $P_E$ while providing a hydrogen plant with electricity $P_{EH2}$ and thermal energy $P_{TH2}$, see the diagram in Figure 6.6. $\beta$ and $\gamma$ determine the distribution of the reactor thermal power $P_{th}$ into $P_E$, $P_{EH2}$, and $P_{TH2}$, see Equations 6.17 to 6.22.

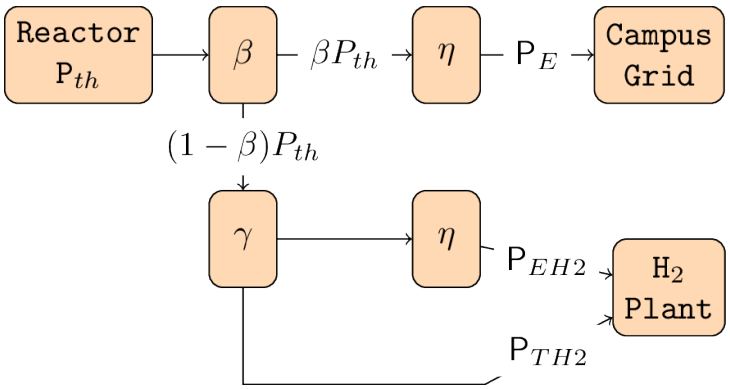


Figure 6.6: Diagram of a reactor coupled to a hydrogen plant.

$$P_E = \eta\beta P_{th} \tag{6.17}$$

$$P_{EH2} = \eta\gamma(1-\beta)P_{th} \tag{6.18}$$

$$P_{TH2} = (1-\gamma)(1-\beta)P_{th} \tag{6.19}$$

where

$$\eta = \text{thermal-to-electric conversion efficiency} \tag{6.20}$$

$$\beta = \frac{P_E/\eta}{P_E/\eta + P_{TH2}/(1-\gamma)} \tag{6.21}$$

$$\gamma = \frac{P_{EH2}/\eta}{P_{EH2}/\eta + P_{TH2}}. \tag{6.22}$$

If $\beta = 1$, the reactor only supplies the grid with electricity $P_E$, and the hydrogen plant does not produce $H_2$. If $\beta = 0$, the reactor only supplies the hydrogen plant, and no electricity goes into the grid. Table 6.1 summarizes the values that $\gamma$ takes for the different methods.

| Method | $\gamma$ | $P_{EH2}$ | $P_{TH2}$ |
|---|---|---|---|
| LTE | 1 | $\neq 0$ | 0 |
| HTE | $0 < \gamma < 1$ | $\neq 0$ | $\neq 0$ |
| SI | 0 | 0 | $\neq 0$ |

Table 6.1: Energy requirements of the different methods.

## 6.7 Results

This section holds the results of the different analyses.

### 6.7.1 Transportation

This subsection centers its focus on the transportation sector. Figure 6.7 displays the fuel consumed per day by MTD and UIUC fleet. Using the values shown in Table 6.2, we calculate the $H_2$ requirement for MTD and UIUC fleets, Figure 6.8. Table 6.3 summarizes the results.

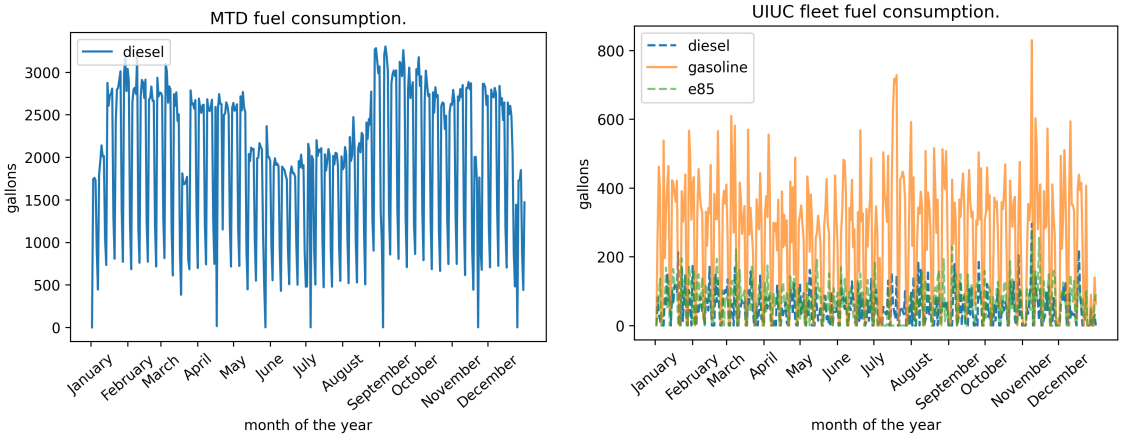


(a) MTD fleet. Data go from July 1, 2018, until June 30, 2019 [15]. (b) UIUC fleet. Data go from January 1, 2019, until December 31, 2019 [58].

Figure 6.7: Fuel consumption data.

Table 6.2: $H_2$ necessary to replace a gallon of fuel [45] [13].

| | Hydrogen Mass [kg] |
|---|---|
| Gasoline | 1 |
| Diesel | 1.13 |
| E85 | 0.78 |

Table 6.3: $H_2$ requirement for MTD and UIUC fleets.

| | |
|---|---|
| Total [tonnes/year] | 943 |
| Average [kg/day] | 2584 |
| Average [kg/h] | 108 |
| Maximum in one day [kg] | 4440 |

Using Table 6.4, we calculate the $CO_2$ savings caused by replacing all the fossil fuels by $H_2$. Table 6.5 displays the $CO_2$ savings for both fleets.

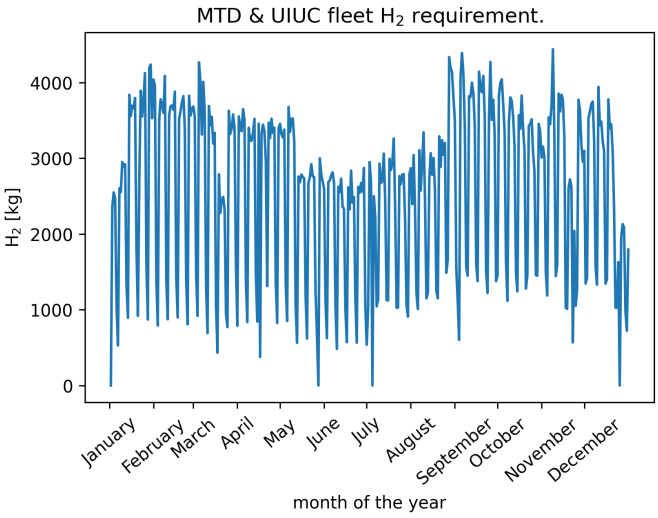


Figure 6.8: $H_2$ requirement for MTD and UIUC fleets.

Table 6.4: $CO_2$ savings in lbs per gallon of fuel burned [1].

| | $CO_2$ produced [lbs/gallon] |
|---|---|
| Gasoline | 19.64 |
| Diesel | 22.38 |
| E85 | 13.76 |

Table 6.5: $CO_2$ yearly savings.

| | $CO_2$ mass [tonnes/year] |
|---|---|
| MTD | 7306 |
| UIUC | 1143 |
| Total | 8449 |

We have determined the $H_2$ requirement by the fleets, and now we seek a microreactor design capable of meeting such demand. For our analysis, we chose a few microreactor designs summarized in Table 6.6. Further studies could include other designs as well.

Figure 6.9 shows the hourly production rates for the different reactors and the $H_2$ production processes. The figure includes a continuous line that represents the hydrogen requirement of both fleets. Note that the SI process' required high temperatures allow for the coupling with only one microreactor design, which has an outlet temperature of more than 800°C.

Table 6.6: Microreactor designs.

| Reactor | P[MWt] | $T_o$[°C] |
|---|---|---|
| MMR [57] | 15 | 640 |
| eVinci [25] | 5 | 650 |
| ST-OTTO [23] | 30 | 750 |
| U-battery [14] | 10 | 750 |
| Starcore [43] | 36 | 850 |

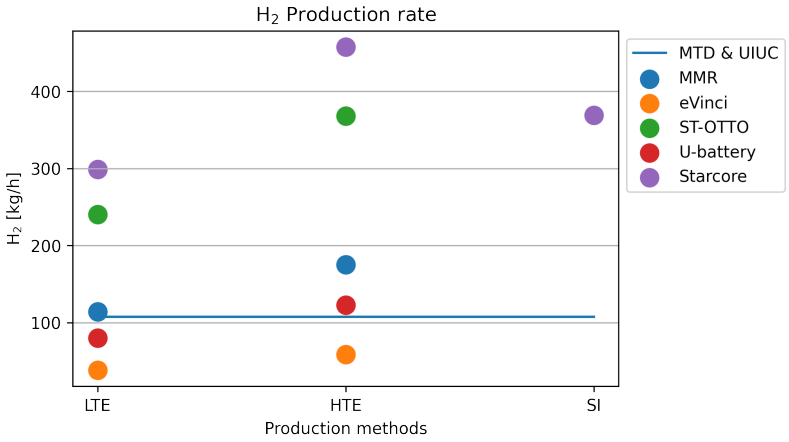


Figure 6.9: Hydrogen production rate by the different microreactor designs.

### 6.7.2 Electricity Generation

This subsection centers its focus on the electricity generation sector and the duck curve problem. To quantify the duck curve's magnitude, we have to predict the UIUC grid's load and the expected electricity production from solar. As the iCAP's main objective is to become carbon neutral before 2050, we make our prediction for that year. UIUC solar farm is relatively new, and the data available is not enough for producing a reliable forecast. To go around this barrier, we use the available data for the whole US. Figure 6.10 displays the prediction for 2050. We carry out the prediction using a linear regression that produces the worst-case scenario. In such a scenario, the total load does not increase considerably, whereas the solar generation does.

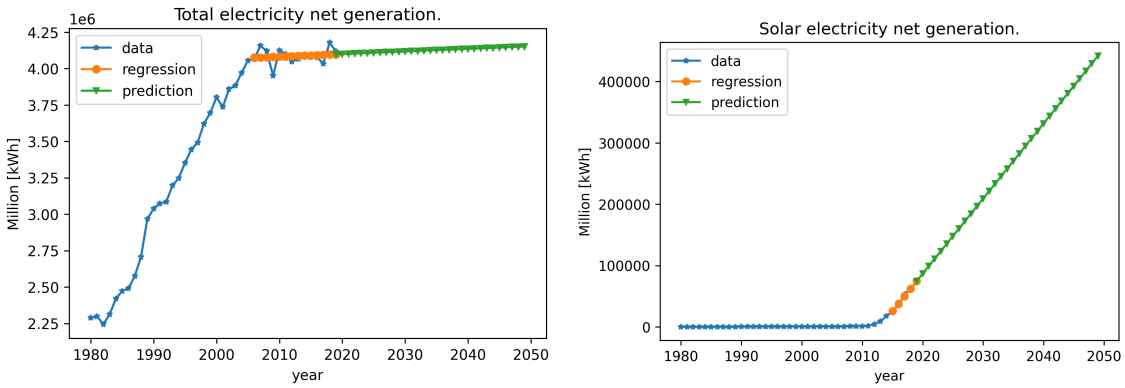


(a) Total electricity generation.

(b) Solar electricity generation.

Figure 6.10: Prediction of the electricity generation in the US for 2050. Data from [2].

The next step was to apply the same growth factor from the predictions to the UIUC grid's load and solar electricity. To obtain a prediction for 2050, we apply the growth factor to the hourly data. We choose a spring day when solar production is higher, as it is sunny, but the total load is low since people are not using electricity for air conditioning or heating [44]. Finally, we subtract the solar production from the total load, obtaining the net load or demand ($D_{NET}$).

We narrowed our analysis' focus to April 4th, when the net demand reached the lowest value in the 2019's spring. Figure 6.11 shows these results. In 2050, the peak net demand will be 46.9 MWh at 5 PM. The lowest net demand will be 15 MWh at 11 AM. These results yield a demand ramp of 31.9 MWh in 4 hours. These results show that the grid requires an available capacity of dispatchable sources of at least 31.9 MW.

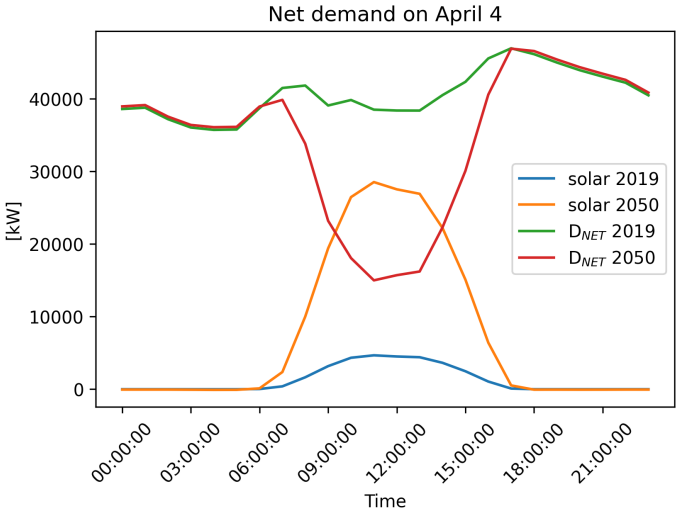


Figure 6.11: Prediction of UIUC's net demand for 2050.

Once we calculated the net demand, the next step was to figure the over-generated electricity. For that purpose,

we arbitrarily chose a reactor of 25 MW. For the LTE case, any reactor is a valid option. We chose an $\eta$ of 33%, which yields a reactor power of 75.8 MWt. For the HTE case, the reactor's choice is an HTGR with an outlet temperature of 850°C. We consider an $\eta$ of 49.8%, which yields a reactor of 50.2 MWt.

The reactor operates at full capacity at all times. However, the reactor electricity ($P_E$) equals the net demand ($D_{NET}$) once smaller than 25 MW. Note that $P_E$ has power units while $D_{NET}$ has energy units. We chose time steps of 1 hour for our analysis, hence $P_E$ and $D_{NET}$ differ by the constant $h$. As $P_E$ is lower than 25 MW, and the reactor is at full thermal capacity, the hydrogen plant takes the excess of thermal energy. We use equation 6.23 with equations 6.17 to 6.22 to calculate the hydrogen produced. Figure 6.12 displays the results. The total $H_2$ production reaches 660, 1009, and 815 kg for LTE, HTE, and SI.

$$\begin{aligned} P_E &= D_{NET} \\ \frac{P_E}{25MW} &= \frac{\eta\beta P_{th}}{\eta P_{th}} = \beta \end{aligned} \tag{6.23}$$

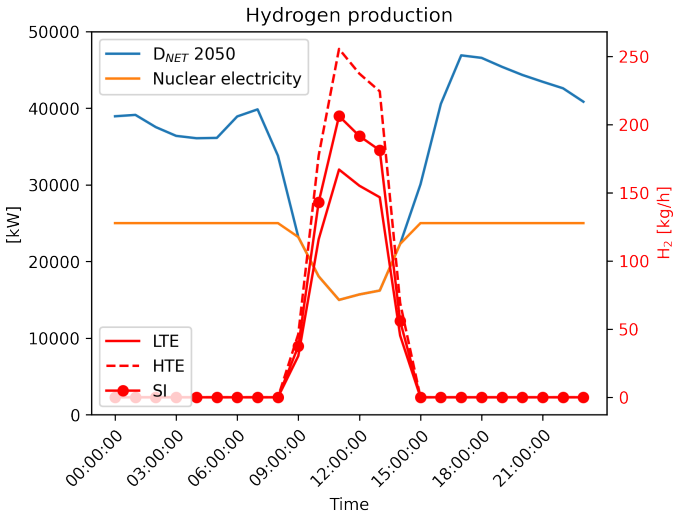


Figure 6.12: $H_2$ production.

Our analysis last step is to calculate the peak demand reduction by using the hydrogen to produce electricity. The energy produced by hydrogen is $285 kJ/mol$, equal to 40 kWh/kg [54]. However, conventional fuel cells can use up to 60% of that energy [19]. Knowing the mass of hydrogen produced, we calculate the total electricity produced. We now reduce the peak demand by distributing the electricity over a specific range of hours. We chose to distribute the electricity for over 6 hours. We calculate the new peak using equation 6.25. Figure 6.13 shows these results. The different $H_2$ processes can generate 15.84 MWh, 24.2 MWh, and 19.6 MWh, respectively. This generation accounts

for a peak reduction of 5 MW, 6.4 MW, and 5.6 MW, respectively.

$$NP = \frac{\sum_{i=0}^{N} D_{NET,i} - TH}{N} \tag{6.24}$$

(6.25)

where

$$NP = \text{New peak magnitude} \tag{6.26}$$

$$D_{NET,i} = \text{Hourly net demant} \tag{6.27}$$

$$TH = \text{Total mass oh hydrogen} \tag{6.28}$$

$$N = \text{Total number of hours when we use the } H_2 \tag{6.29}$$

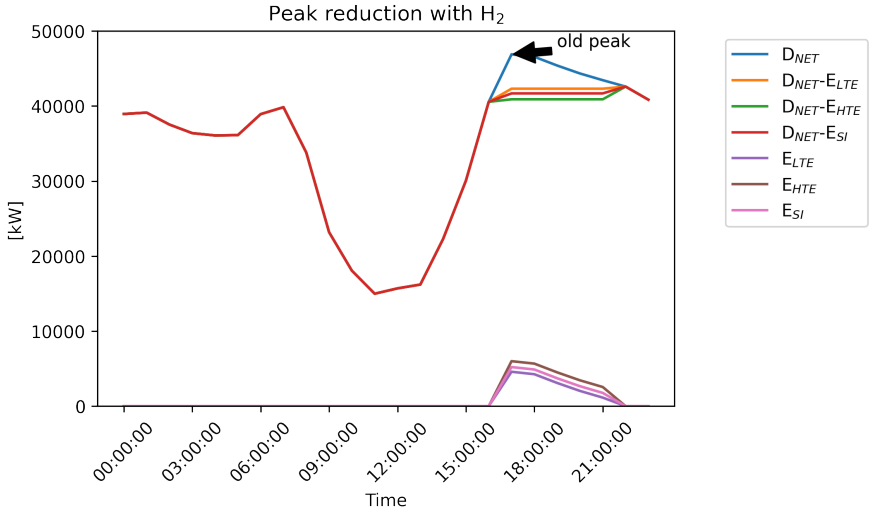


Figure 6.13: Peak reduction by using the produced $H_2$.

## 6.8 Conclusions

The world faces energy challenges that compromise the efforts to stop climate change. The electricity generation and transportation sectors are the largest issuers of GHGs and, hence, the major contributors to climate change. These challenges underscore the need for cleaner sources. Nonetheless, the common belief that renewable energy is the solution to the problem presents several drawbacks. The duck curve is an example of such drawbacks. Moreover,

a carbon-neutral electric grid will be insufficient to halt climate change. The transportation sector needs to survey some possible alternatives to become carbon-free as well. In this work, we proposed combining nuclear energy and hydrogen production that represents a possible solution to these challenges.

To seek a solution for the challenge described above, we narrowed down our focus on a more particular case, the University of Illinois. Through the implementation of the iCAP, the University of Illinois is actively working to reduce GHG emissions on its campus. This work's objective aligns with the efforts in two of the six target areas defined on the iCAP, electricity generation, and transportation.

Regarding hydrogen production methods, we surveyed three different processes: LTE, HTE, and SI. We developed a tool to calculate their energy requirements, regarding electricity and heat, and hydrogen production rates. This tool is applicable to a stand-alone hydrogen plant and a nuclear power plant that produces both electricity and hydrogen.

In the transportation sector analysis, we quantified the fuel requirements of MTD and UIUC fleets. We calculated the mass of hydrogen necessary to replace 100% of the fleet's fossil fuel usage. Finally, we chose several microreactor designs, and we calculated their hydrogen production rates. The microreactors that can meet both fleet hydrogen needs are the MMR, ST-OTTO, U-battery, and Starcore. Starcore design is the only one that could use the SI process.

In the electricity generation sector analysis, we predicted the duck curves' magnitude in UIUC's grid in 2050. This result exhibits how an increased solar penetration into the grid worsens the duck curve. We proposed a mitigation strategy that uses a microreactor of 25 MWe. For such a reactor, we calculated the mass of hydrogen produced by the different methods during the day. Finally, we estimated a peak demand reduction by using the hydrogen produced during the day. This last result highlights that hydrogen introduces a means to store energy that reduces the reliance on dispatchable sources. This analysis emphasizes how nuclear energy and hydrogen production are an approach to mitigate climate change.

# Chapter 7

# Conclusions

## 7.1 Contribution

This section will summarize the contributions of this thesis.

## 7.2 Future Work

This section will introduce some possible future work as a continuation of this thesis.

# Appendix

Appendix.

# References


[1] Administration, E. I. (2014). How much carbon dioxide is produced by burning gasoline and diesel fuel?

[2] Administration, U. E. I. (2020). Electric Power Monthly with data for February 2020. page 273.

[3] Association, W. N. (2020). Small nuclear power reactors - World Nuclear Association.

[4] Balay, Brune, Buschelman, Gropp, Karpeyev, Knepley, McInnes, C., Rupp, Smith, and Zhang (2016). PETSc Users Manual.

[5] Ballinger, R. G., Wang, C. Y., Kadak, A., Todreas, N., Mirick, B., Demetri, E., and Koronowski, M. (2004). Balance of Plant System Analysis and Component Design of Turbo-Machinery for High Temperature Gas Reactor Systems. Technical Report 828709.

[6] Benjamin Russ (2009). Sulfur Iodine Process Summary for the Hydrogen Technology Down-Selection. Technical Report INL/EXT-12-25773, 1047207.

[7] Bostelmann, F., Hammer, H. R., Ortensi, J., Strydom, G., Velkov, K., and Zwermann, W. (2016). Criticality calculations of the Very High Temperature Reactor Critical Assembly benchmark with Serpent and SCALE/KENO-VI. *Annals of Nuclear Energy*, 90:343–352.

[8] Bouillon, B. (2014). Prepared Statement of Brad Bouillon on behalf of the California Independent System Operator Corporation.

[9] Breeze, P. (2014). Nuclear Power. In *Power Generation Technologies*, pages 353–378. Elsevier.

[10] Brey, H. (2001). Development History of the Gas Turbine Modular High Temperature Reactor.

[11] Brown, L., Besenbruch, G., Lentsch, R., Schultz, K., Funk, J., Pickard, P., Marshall, A., and Showalter, S. (2003). HIGH EFFICIENCY GENERATION OF HYDROGEN FUELS USING NUCLEAR POWER. Technical report, GENERAL ATOMICS (US).

[12] Burke, P. J., Stern, D. I., and Bruns, S. B. (2018). The Impact of Electricity on Economic Development: A Macroeconomic Perspective. *International Review of Environmental and Resource Economics*, 12(1):85–127.

[13] Center, A. F. D. (2014). Fuel Properties Comparison.

[14] Ding, M., Kloosterman, J. L., Kooijman, T., and Linssen, R. (2011). Design of a U-Battery. Technical Report PNR-131-2011-014, Urenco, and Koopman and Witteveen.

[15] District, C.-U. M. T. (2019). Champaign-Urbana Mass Transit District Public Records.

[16] Dotson, S. G. and Huff, K. D. (2020). Optimal Sizing of a Micro-Reactor for Embedded Grid Systems. In *Transactions of the American Nuclear Society Student Conference*, Raleigh, N.C. American Nuclear Society.

[17] Duderstadt, J. J. and Hamilton, L. J. (1976). *Nuclear Reactor Analysis*. Wiley, New York, 1 edition edition.

[18] El-Shafie, M., Kambara, S., and Hayakawa, Y. (2019). Hydrogen Production Technologies Overview. *Journal of Power and Energy Engineering*, 07(01):107–154.

[19] Energy, D. E. E. a. R. (2015). Fuel cells fact sheet.

[20] EPA, U. (2020). Sources of Greenhouse Gas Emissions.

[21] Gaston, D., Newman, C., Hansen, G., and Lebrun-Grandié, D. (2009). MOOSE: A parallel computational framework for coupled systems of nonlinear equations. *Nuclear Engineering and Design*, 239(10):1768–1778.

[22] Hales, J., Williamson, R., Novascone, S., Perez, D., Spencer, B., and Pastore, G. (2013). Multidimensional multiphysics simulation of TRISO particle fuel. *Journal of Nuclear Materials*, 443(1-3):531–543.

[23] Harlan, B. (2018). X-energy Xe-100 Reactor initial NRC meeting.

[24] HELMETH (2020). High temperature electrolysis cell (SOEC).

[25] Hernandez, R., Todosow, M., and Brown, N. R. (2019). Micro heat pipe nuclear reactor concepts: Analysis of fuel cycle performance and environmental impacts. *Annals of Nuclear Energy*, 126:419–426.

[26] Herranz, L., Linares, J., and Moratilla, B. (2009). Power cycle assessment of nuclear high temperature gas-cooled reactors. *Applied Thermal Engineering*, 29(8-9):1759–1765.

[27] Huning, A. J. (2014). A STEADY STATE THERMAL HYDRAULIC ANALYSIS METHOD FOR PRISMATIC GAS REACTORS.

[28] IAEA (2001). Current status and future development of modular high temperature gas cooled reactor technology.

[29] J. E. O'Brien, C. M. Stoots, J. S. Herring, M. G. McKellar, E. A. Harvego, M. S. Sohal, and K. G. Condie (2010). High Temperature Electrolysis for Hydrogen Production from Nuclear Energy TechnologySummary. Technical Report INL/EXT-09-16140, 978368.

[30] Kalamaras, C. M. and Efstathiou, A. M. (2013). Hydrogen Production Technologies: Current State and Future Developments. *Conference Papers in Energy*, 2013:1–9.

[31] Kirk, B. S., Peterson, J. W., Stogner, R. H., and Carey, G. F. (2006). libMesh : a C++ library for parallel adaptive mesh refinement/coarsening simulations. *Engineering with Computers*, 22(3-4):237–254.

[32] Knoll, D. and Keyes, D. (2004). Jacobian-free Newton–Krylov methods: a survey of approaches and applications. *Journal of Computational Physics*, 193(2):357–397.

[33] Leppänen, J. (2007). Development of a New Monte Carlo Reactor Physics Code. page 241.

[34] Leppänen, J., Aufiero, M., Fridman, E., Rachamin, R., and van der Marck, S. (2014). Calculation of effective point kinetics parameters in the Serpent 2 Monte Carlo code. *Annals of Nuclear Energy*, 65:272–279.

[35] Lindsay, A., Ridley, G., Rykhlevskii, A., and Huff, K. (2018). Introduction to Moltres: An application for simulation of Molten Salt Reactors. *Annals of Nuclear Energy*, 114:530–540.

[36] MacDonald, P. E. (2003). NGNP Preliminary Point Design – Results of the Initial Neutronics and Thermal-Hydraulic Assessments. page 118.

[37] Melese, G. and Katz, R. (1984). *Thermal and flow design of helium-cooled reactors*. American Nuclear Society, La Grange Park, Ill., USA.

[38] Ming, Z., Olson, A., Jiang, H., Mogadali, M., and Schlag, N. (2019). Resource Adequacy in the Pacific Northwest.

[39] Nagashima, M. and Institut français des relations internationales (2018). *Japan's hydrogen strategy and its economic and geopolitical implications*. OCLC: 1059514336.

[40] NEA, O. (2017). Benchmark of the Modular High-Temperature Gas-Cooled Reactor (MHTGR)-350 MW Core Design Volumes I and II. page 110.

[41] Neylan, A., Graf, D., and Millunzi, A. (1988). The modular high temperature gas-cooled reactor (MHTGR) in the U.S. *Nuclear Engineering and Design*, 109(1-2):99–105.

[42] Novak, A. J., Zou, L., Peterson, J. W., Martineau, R. C., and Slaybaugh, R. N. (2018). Pronghorn: A Porous Media Thermal-Hydraulics Core Simulator and its Validation with the SANA Experiments.

[43] Nuclear, S. C. (2015). Star Core Spec Sheet.

[44] of Energy, U. D. (2017). Confronting the Duck Curve: How to Address Over-Generation of Solar Energy.

[45] of Energy Efficiency and Renewable Energy, D. O. (2020). Hydrogen Production Processes. Library Catalog: www.energy.gov.

[46] of Illinois at Urbana-Champaign, U. (2015). Illinois Climate Action Plan.

[47] O'Brien, J. E., Herring, J. S., Stoots, C. M., McKellar, M. G., Harvego, E. A., Condie, K. G., Housley, G. K., and Hartvigsen, J. J. (2019). Status of the INL High- Temperature Electrolysis Research Program – Experimental and Modeling. page 13.

[48] Park, H., Knoll, D. A., Gaston, D. R., and Martineau, R. C. (2010). Tightly Coupled Multiphysics Algorithms for Pebble Bed Reactors. *Nuclear Science and Engineering*, 166(2):118–133.

[49] Ragusa, J. C. and Mahadevan, V. S. (2009). Consistent and accurate schemes for coupled neutronics thermal-hydraulics reactor analysis. *Nuclear Engineering and Design*, 239(3):566–579.

[50] Rohde, U., Baier, S., Duerigen, S., Fridman, E., Kliem, S., and Merk, B. (2012). Development and verification of the coupled 3D neutron kinetics/thermal-hydraulics code DYN3D-HTR for the simulation of transients in block-type HTGR. *Nuclear Engineering and Design*, 251:412–422.

[51] Silady, F., Cunliffe, J., and Walker, L. (1988). The licensing experience of the Modular High-Temperature Gas-Cooled Reactor (MHTGR). *Energy*, 16(1-2):417–424.

[52] Tak, Kim, Lim, and Noh (2012). A practical method for Whole-Core Thermal Analysis of a Prismatic Gas-Cooled Reactor.

[53] Tak, N.-i., Kim, M.-H., and Lee, W. J. (2008). Numerical investigation of a heat transfer within the prismatic fuel assembly of a very high temperature reactor. *Annals of Nuclear Energy*, 35(10):1892–1899.

[54] Ursua, A., Gandia, L. M., and Sanchis, P. (2012). Hydrogen Production From Water Electrolysis: Current Status and Future Trends. *Proceedings of the IEEE*, 100(2):410–426.

[55] US-DOE (2019). The Ultimate Fast Facts Guide to Nuclear Energy. Fact Sheet DOE/NE-0150, Department of Energy Office of Nuclear Energy, Washington D.C. https://www.energy.gov/ne/downloads/ultimate-fast-facts-guide-nuclear-energy.

[56] USDRIVE (2017). Hydrogen Production Tech Team Roadmap.

[57] USNC (2019). MMR - USNC.

[58] Varney, P. (2020). Personal Communication.

[59] White, F. (2006). *Viscous Fluid Flow*. McGraw Hill, third edition.

[60] Yildiz, B. and Kazimi, M. (2006). Efficiency of hydrogen production systems using alternative nuclear energy technologies. *International Journal of Hydrogen Energy*, 31(1):77–92.